DRUG DELIVERY
2020, VOL. 27, NO. 1, 642–651
https://doi.org/10.1080/10717544.2020.1754524

Taylor & Francis
Taylor & Francis Group

RESEARCH ARTICLE

OPEN ACCESS Check for updates

Polyvinylpyrrolidone microneedles for localized delivery of sinomenine hydrochloride: preparation, release behavior of *in vitro* & *in vivo,* and penetration mechanism

Zixuan Shu[a]*, Yingji Cao[a]*, Yaotian Tao[a,b,c], Xiao Liang[a], Fangyuan Wang[a], Zhi Li[a], Zhenbao Li[a,b,c] and Shuangying Gui[a,b,c,d]

[a]College of Pharmacy, Anhui University of Chinese Medicine, Hefei, Anhui, China; [b]Institute of Pharmaceutics, Anhui Academy of Chinese Medicine, Hefei, Anhui, China; [c]Engineering Technology Research Center of Modernized Pharmaceutics, Anhui Education Department (AUCM), Hefei, Anhui, China; [d]Anhui Province Key Laboratory of Chinese Medicine Research and Development, Anhui University of Chinese Medicine, Hefei, Anhui, China

ABSTRACT

Sinomenine (SIN) is an anti-inflammatory alkaloid derived from *Sinomenium acutum*, and the products sinomenine hydrochloride (SH) tablets and injections have been marketed in China to treat rheumatoid arthritis (RA). Oral administration of SH has shortcomings of gastrointestinal irritation and low bioavailability. The injection may require professional training and higher cost. It is of interest to develop an alternative form that is easier to administer and avoids the first-pass metabolism. In this study, SH-loaded dissolving microneedles (SH-MN) were fabricated using polyvinyl pyrrolidone and chondroitin sulfate with a casting method. In percutaneous permeation studies of *In vitro,* the cumulative permeation and permeation rate of SH-MN were 5.31 and 5.06 times higher than that of SH-gel (SH-G). In percutaneous pharmacokinetic studies, the values of the area under the curve after administration of SH-MN in the skin and blood were 1.43- and 1.63-fold higher than that of SH-G, respectively. In percutaneous absorption studies, SH-MN could absorb into tissue fluid; and dissolve after skin penetration. The drug was released along the channel and spread to surrounding skin tissue. After 4 h, the needle tip was almost completely dissolved, and the drug could penetrate to a depth of 200 μm under the skin. These results demonstrate that the SH-MN is an effective, safe, and simple strategy for transdermal SH delivery.

ARTICLE HISTORY
Received 8 February 2020
Revised 30 March 2020
Accepted 7 April 2020

KEYWORDS
Sinomenine hydrochloride; dissolving microneedles; transdermal drug delivery system; microdialysis; fluorescent labeling

1. Introduction

Sinomenine (SIN) is a bioactive alkaloid derived from the roots and stems of the plant *Sinomenium acutum* (Garcia et al., 2016) that has antiarthritis (Gao et al., 2018), antiapoptosis (Chen et al., 2017), and immunosuppressive (Gao et al., 2019) effects. The structure of SIN is shown in Figure 1. It is normally used as sinomenine hydrochloride (SH) in clinical practice. However, oral SH can cause adverse reactions such as gastrointestinal irritation and a first-pass effect. Injections are more expensive and require professional training for administration (Wu et al., 2016; Arya et al., 2017). Transdermal drug delivery is an attractive alternative to oral administration or injection, and early studies confirmed that it could overcome the above-mentioned problems (Prausnitz & Langer, 2008; Romgens et al., 2015).

Transdermal drug delivery can prevent the first-pass effect and gastrointestinal tract irritation, reduce dosing frequency, and maintain blood concentrations for a sustained-release effect (Liu et al., 2019; Zhao et al., 2016). Transdermal drug delivery systems are usually limited by the human skin barrier, especially the stratum corneum (Van Smeden et al., 2014). Molecules that can be delivered by the transdermal route are restricted to small (<500 Da) and moderately sized hydrophobic agents (Fernandez-Garcia et al., 2020; Yin et al., 2019). To address this challenge, researchers designed a variety of external stimuli methods to promote percutaneous drug absorption. These external triggers include iontophoresis, ultrasonic introduction, electroporation, and thermal perforation (Jabbari et al., 2015; Ita, 2016; Lopez-Ramirez et al., 2020). However, these methods can cause pain, and patients cannot administer the compounds by themselves. How to effectively overcome the barrier of the stratum corneum has become a key issue in the research of transdermal SIN preparations.

Microneedles (MN) have become an attractive platform to overcome the skin barrier for cutaneous drug delivery in an almost noninvasive manner (Henry et al.,1998; Fakhraei et al., 2018; Kim et al., 2018; Kiselmann et al., 2018; Boopathy et al., 2019). MN are an array of needles miniaturized down to the

CONTACT Zhenbao Li lizhenbao@ahtcm.edu.cn; Shuangying Gui guishy0520@126.com College of Pharmacy, Anhui University of Chinese Medicine, Hefei, Anhui, China
*These authors made equal contributions to this work.

micrometer scale. They were initially used for transdermal delivery of drugs and vaccines because of they are pain-free, risk-free, and easy to use (Kaushik et al., 2001; Sullivan et al., 2010; Kim et al., 2014; Chang et al., 2017; Xu et al., 2017). Indeed, MN can avoid unnecessary pain during cutaneous administration by taking advantage of their length: they are sufficient to pierce skin but not long enough to stimulate dermal nerves (Arya et al., 2017; Ma & Wu, 2017). Dissolving MN have received increasing attention owing to their ease of preparation and improved safety. Unlike hollow and solid MN, dissolving MN are mainly composed of water-soluble sugars and polymers. When they contact moisture in the intradermal region, the needle tips dissolve rapidly to allow damaged skin recovery and minimize the risk of infection (Hong et al., 2013).

In this study, we selected polyvinyl pyrrolidone and chondroitin sulfate as matrix materials to prepare SH-MN, and the percutaneous permeability of drug-loaded MN was investigated. A microdialysis sampling technique was used to assess the distribution and concentration of SIN in rats over time. The MN with SIN fluorescent labels were used to investigate skin release and drug distribution. The transdermal mechanism of MN was studied to provide an experimental basis for further study of drug-loaded MN.

2. Methods

2.1. Materials and animals

SH (purity >98%) was purchased from GuanYu Biological Technology Co., Ltd. (Shanxi, China). SH reference substance was purchased from the China Pharmaceutical Biological Products Analysis Institute (Beijing, China). Chondroitin sulfate was supplied by LvShengYuan Technology Co., Ltd. (Beijing, China). Polyvinylpyrrolidone was purchased from Xilong Chemical Co., Ltd. (Guangdong, China). Sodium sulfide was purchased from Chemical industry Co., Ltd. (WuXi, China). Methylene blue was supplied by Guangzhou Chemical Co., Ltd. (Guangdong, China). Methanol and triethylamine were obtained from Xingke Solvents Co., Ltd. (Shanghai, China). Water was distilled and passed through a Milli-Q water purification system (Millipore, Burlington, MA, USA). All other reagents were of analytical grade or pharmaceutical grade.

Male Sprague Dawley rats (200 ± 10 g, 6–8 weeks-old) were provided by the Experimental Animal Center of Anhui Medical University (Anhui, China). All animal experiments were conducted in accordance with the guidelines of the Laboratory Animal Center of Anhui University of Chinese Medicine. All animal experiments were performed in compliance with the animal Management Rules of the Ministry of Health of the People's Republic of China (Jinan, China, Approval No. 1107261911002543).

2.2. SH-MN preparation and characterization

2.2.1. Preparation of SH-MN

SH-MN were formulated by a casting method. The ingredients are listed in Table 1. Briefly, PVP, CS, and SH were dissolved in water (50 mL). The mixture was stirred for 10 min, then the uniform solution was poured into the MN mold (7 × 10 array of microneedles, made of Poly tetra fluoroethylene) and vacuumized at 25 °C under a pressure of −70 kPa for 15 min. Next, it was placed in a desiccator and dried at room temperature for 48 h. The MN mold is prepared by mechanical punching on a polytetrafluoroethylene plate.

Table 1. SH-MN compositions.

Formulation	PVP (wt%)	CS (wt%)	SH (wt%)
F1	40	40	20
F2	35	35	30
F3	33	32	35
F4	30	30	40
F5	50	30	20
F6	50	20	30
F7	50	15	35
F8	50	10	40

2.2.2. SH-MN morphology

The morphologies and dimensions of the fabricated MN were observed by optical microscopy (model XP-330C, Caikon Co., Shanghai, China).

2.2.3. Mechanical testing of SH-MN

The Mechanical testing of SH-MN was tested by insertion into rat abdomen skin. Briefly, a rat was sacrificed, and a piece of abdomen skin was shaved, cut off, and cleaned with distilled water. The prepared MN were inserted into excised rat skins with a force of 5 N for 3 min and then peeled off. The skin was immediately stained with methylene blue solution, washed with isopropyl alcohol reagent, and the skin was observed with optical microscopy (Wang et al., 2017).

2.3. Quantification of in vitro release from SH-MN

A modified Franz diffusion cell (TK-6A, Shanghai Yukai Technology Trade Co., Ltd., Shanghai, China) was used to investigate the *in vitro* diffusion of MN prepared in diffusion of SH from different MN formulations. The drug-loaded MN were used to puncture the skin with a force of 5 N and remained in the skin, which was then fixed onto Franz diffusion cells with the stratum corneum side facing the supply room. The receiving room was filled with 8 mL of phosphate-buffered saline (PBS, pH 6.8), stirring at the speed of 120 rpm at 37 °C. Then, 1.0 mL of the sample was removed from the receiving room at the defined time points of 0.17, 0.5, 1, 2, 4, 6, 10, 12, and 24 h, while supplementing an equal volume of isothermal PBS. The concentration of SH in samples was determined by high-performance liquid chromatography (HPLC).

2.4. In vitro percutaneous permeation studies

2.4.1. Preparation of SH-gel (SH-G)

2.0 g of Carbomer 940 was dispersed into 100.0 mL of distilled water with stirring to form a homogeneous solution.

Next, 4.0 g of SH dissolved with 20.0 mL of ethanol was carefully added to the swelling carbomer matrix under stirring. Finally, the pH was adjusted to 7.0 with triethanolamine.

2.4.2. In vitro *percutaneous permeation of SH-MN and SH-G*

According to the previous method, SH-MN and SH-G were fixed or daubed on the skin to measure their *in vitro* percutaneous permeation.

2.5. HPLC analysis

The Ultimate 3000 HPLC system (Thermo Fisher Scientific, Waltham, MA) was used to analyze the samples and determine the concentrations of SH with a Thermo syncronis C18 column (250 mm × 4.6 mm, 5.0 μm). The mobile phase consisted of methanol and water containing 0.075% phosphate and 0.125% triethylamine with a flow rate of 1.0 mL/min (18:32, pH = 3). The column was kept constant at 30 °C, and the detection wavelength was 265 nm.

2.6. In vivo *skin-vessel synchronous microdialysis*

Flow rate and concentration are important factors in determining probe recovery. Increment and decrement methods were used to determine probe recovery *in vivo* and *in vitro*.

2.6.1. *Microdialysis system*

The microdialysis apparatus was composed of a syringe pump (CMA 400; CMA Microdialysis Stockholm, Sweden), perfusion apparatus (CMA 2.5 mL), microcollector (CMA 470), and microdialysis probe (MAB7). The probes had a 15-kDa cut off with a 0.6-mm membrane diameter (10 mm in length) and the perfusate was blank Ringer's solution.

2.6.2. *Effect of flow rate and concentration on* in vitro *recovery*

The probe was completely immersed in Ringer's solution containing SH (10 μg mL^{-1}). The temperature was maintained at 37 °C while stirring at 200 rpm. The blank Ringer's solution was perfused at different flow rates of 0.5, 1, 2, and 4 μL min^{-1}. In the other group, the probe was completely immersed in the Ringer's solution containing different concentrations of SH (1, 5, 10, 20 μg mL^{-1}). Stirring was maintained for all conditions. The Ringer's solutions containing SH at different concentrations were used to perfuse the probe at a flow rate of 1 μL min^{-1}. Samples were collected after 1 h of equilibration. The drug content (C_{out}) in the dialysate was determined by UHPLC-tandem mass spectrometry (MS/MS), and the recovery rate of SH was calculated by the increment method:

$$R_i = C_{out}/C_{in}.$$

where R_i is the recovery of probe, C_{in} is the initial concentration, and C_{out} is the concentration after dialysis.

The probes were immersed in blank Ringer's solution at a constant temperature of 37 °C. Ringer's solution containing 10 μg mL^{-1} SH was perfused at four flow rates of 0.5, 1, 2, and 4 μL min^{-1}. The *in vitro* recovery rate of the probes was calculated using the decrement method with the following equation:

$$R_d = (C_{in}–C_{out})/C_{in}.$$

where R_d is the recovery of probes, C_{in} is the initial concentration, and C_{out} is the concentration after dialysis.

2.6.3. *Effect of flow rate and concentration on* in vivo *recovery*

After the probe was implanted, Ringer's solution of SH at 10 μg mL^{-1} was used to perfuse the probe at different flow rates (0.5, 1, 2, and 4 μL min^{-1}). In the other group, the probes were perfused with SH perfusate at different concentrations (1, 5, 10, and 20 μg mL^{-1}) at a flow rate of 1 μL min^{-1}. Samples were collected after 1 h of equilibration. *In vivo* recovery was calculated using the decrement method.

2.6.4. In vivo *probe recovery experiment*

Rats were anesthetized with a dose of 0.5 mL·per 100 g (20%, w/v) urethane by intraperitoneal injection. Throughout the experiment, the rats were kept on a temperature-controlled heating pad to maintain body temperature at 37–38 °C. Prior to probe implantation, the abdominal region was carefully shaved. Then the guide needle was drawn out, and the membrane was left in the implantation region. The microdialysis probes were implanted into the subcutaneous tissue and right jugular vein with the aid of a guide needle. Subsequently, Ringer's solution of SH at 10 μg mL^{-1} was used to perfuse the probe at different flow rates (0.5, 1, 2, and 4 μL min^{-1}). In another group, the probes were pumped with SH perfusate at different concentrations (1, 5, 10, and 20 μg mL^{-1}) at a flow rate of 1 μL min^{-1}. Samples were collected after 1 h of equilibration. *In vivo* recovery was calculated using the same method employed for *in vitro* recovery.

2.6.5. In vivo *pharmacokinetics of SH-MN*

Ten Sprague Dawley rats (190–210 g) were weighed and randomly divided into SH-MN and SH-G groups (5 rats/per group). After the probe was implanted and equilibrated for 1 h, 40 μL of skin and blood blank dialysate were collected. In the SH-MN group, the MN were used to puncture the abdominal skin with 5 N force and then left in the skin. In the SH-G group, the SH-loaded gel was applied to the abdominal skin of rats on an area of 1.0 cm^2 at a dose of 60 mg kg^{-1}. Samples were collected into vials at 40-min intervals.

2.7. UHPLC-MS/MS analysis

SIN in biological samples was analyzed using a validated UHPLC-MS/MS method. The UHPLC-MS/MS system (UHPLC-MS/MS-5500 system, AB Sciex, Framingham, MA) contained

an ExionLCTM AD UHPLC system and a QTRAP 5500 triple quadrupole mass instrument equipped with an electrospray ionization (ESI) source. Data acquisition and analysis were performed using MultiQuantTM software (AB Sciex). Liquid chromatographic separation was carried out at 30 °C using a 1.8-μm, 100 mm × 2.1 mm Epic C18 column. A sample volume of 2 μL was injected at a flow rate of 0.2 mL min^{-1}. Isocratic elution was performed using acetonitrile containing 0.1% (v/v) formic acid and water containing 0.1% (v/v) formic acid (11:89). The ESI source was operated under the positive ionization mode, and the MS conditions were set at: desolvation temperature, 250 °C; heat block temperature, 550 °C; nebulizer gas flow, 3 L min^{-1}; drying gas flow, 15 L min^{-1}; interface voltage, 3.5 KV. Ion pair: SH: *m/z* 330.0 → 181.1, declustered voltage (DP): 98 V, collision energy (CE): 45 eV, inlet voltage (EP): 10 V, collision cell outlet voltage (CXP): 10 V; ion pair: procaine hydrochloride (internal standard) *m/z* 237.0 → 100.2, DP: 50 V, CE: 21 eV, EP: 10 V, CXP: 10 V.

2.8. Penetration mechanism study

2.8.1. Method for preparing fluorescent marker MN

The SIN fluorescent label was synthesized using the method reported in the literature (Pan et al., 2010). SIN and fluorescein isothiocyanate (FITC) served as raw materials, and a FITC fluorescent group was placed in the SIN C-1 position. The chemical structure of the label is shown in Figure 2.

2.8.2. Morphology and mechanical investigation

The morphology and mechanical properties of MN containing fluorescent markers were investigated.

2.8.3. In vivo *release behavior experiment*

Healthy rats were weighed and anesthetized by intraperitoneal injection of 3.5% chloral hydrate (1 mL·per 100 g). The MN containing SIN fluorescent markers were used to puncture the skin in the marked area of the rat abdomen for 3 min with a force of 5 N and stayed in the skin. After administration, the abdomens of rats were wrapped with gauze and fixed with medical tape. The MN were removed 1, 2, 4, and 8 h after administration. The removed MN were imaged by optical microscopy (model XP-330C, Caikon Co., Shanghai, China).

2.8.4. Observation of local skin fluorescence

Rats were sacrificed at 1, 2, 4, and 8 h after administration, and the abdomen skin was cut along the marked administration area. The rat abdomen skin was resected, frozen, and stored at –80 °C until cryo-sectioning. The frozen tissue block was transferred to a cryotome cryostat (–20 °C), and 30-μm longitudinal and 50-μm transverse sections were obtained. The sections were immersed in absolute ethanol for 5 min, then allowed to dry naturally. The longitudinal sections were treated with 4′,6-diamidino-2-phenylindole (DAPI) for 10 min to stain the nuclei. The samples were stored in the dark at

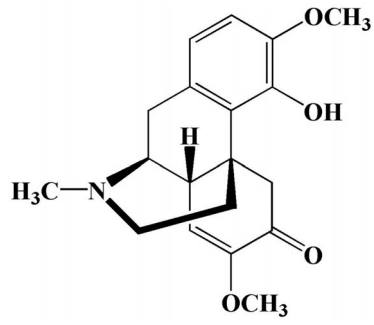

Figure 1. The chemical structure of Sinomenin (Garcia et al., 2016).

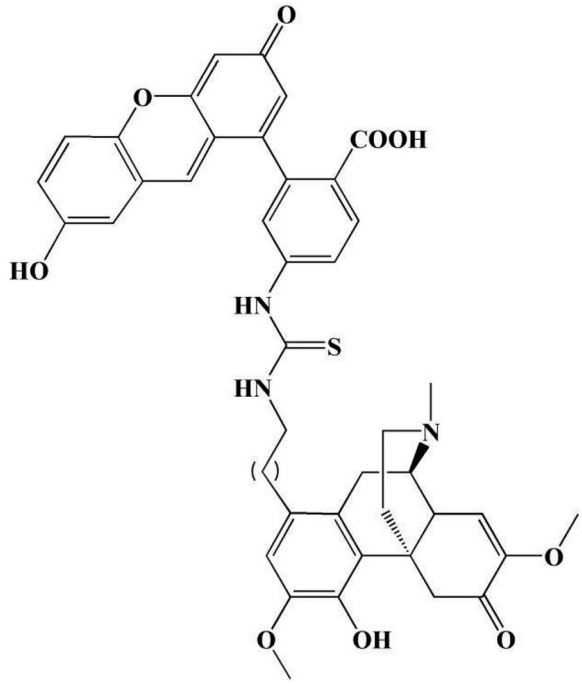

Figure 2. The chemical structure of the SIN fluorescent label.

−20 °C. The longitudinal and transverse tissue sections were observed using a confocal microscope.

2.9. Statistical analysis

All data are expressed as the mean ± SD. Differences between groups were compared by SPSS Statistics 24 (IBM Corp., Armonk, NY) using the independent-samples *t*-tests or paired-samples *t*-tests. Differences were considered statistically significant at $p < .05$ and $p < .01$.

3. Results

3.1. SH-MN characterization

The length of the MN was approximately 0.5 mm, which was sufficient to penetrate the mouse stratum corneum (~5 μm thick) and efficiently deliver SH into the intradermal space. The center-to-center spacing of MN was 1.0 mm. Figure 3 shows that the MN of formulations F1, F2, F5, F6, F7, and F8 were conical, and the needle shapes were clear and complete. The shapes of MN in formulations F3 and F4 were

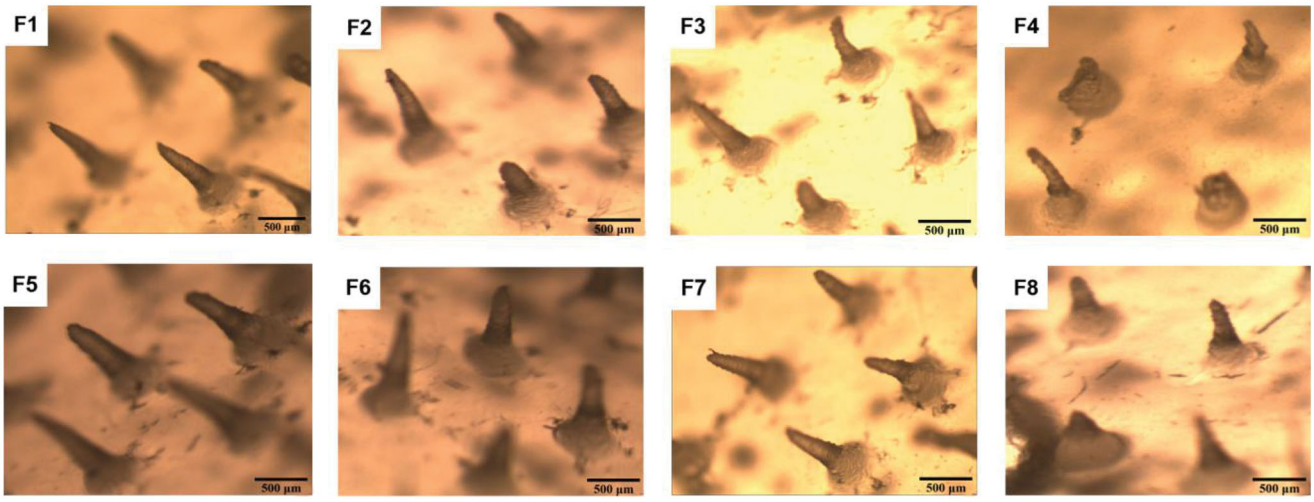

Figure 3. F1–8 are micrographs of SH-MN prepared as different formulations.

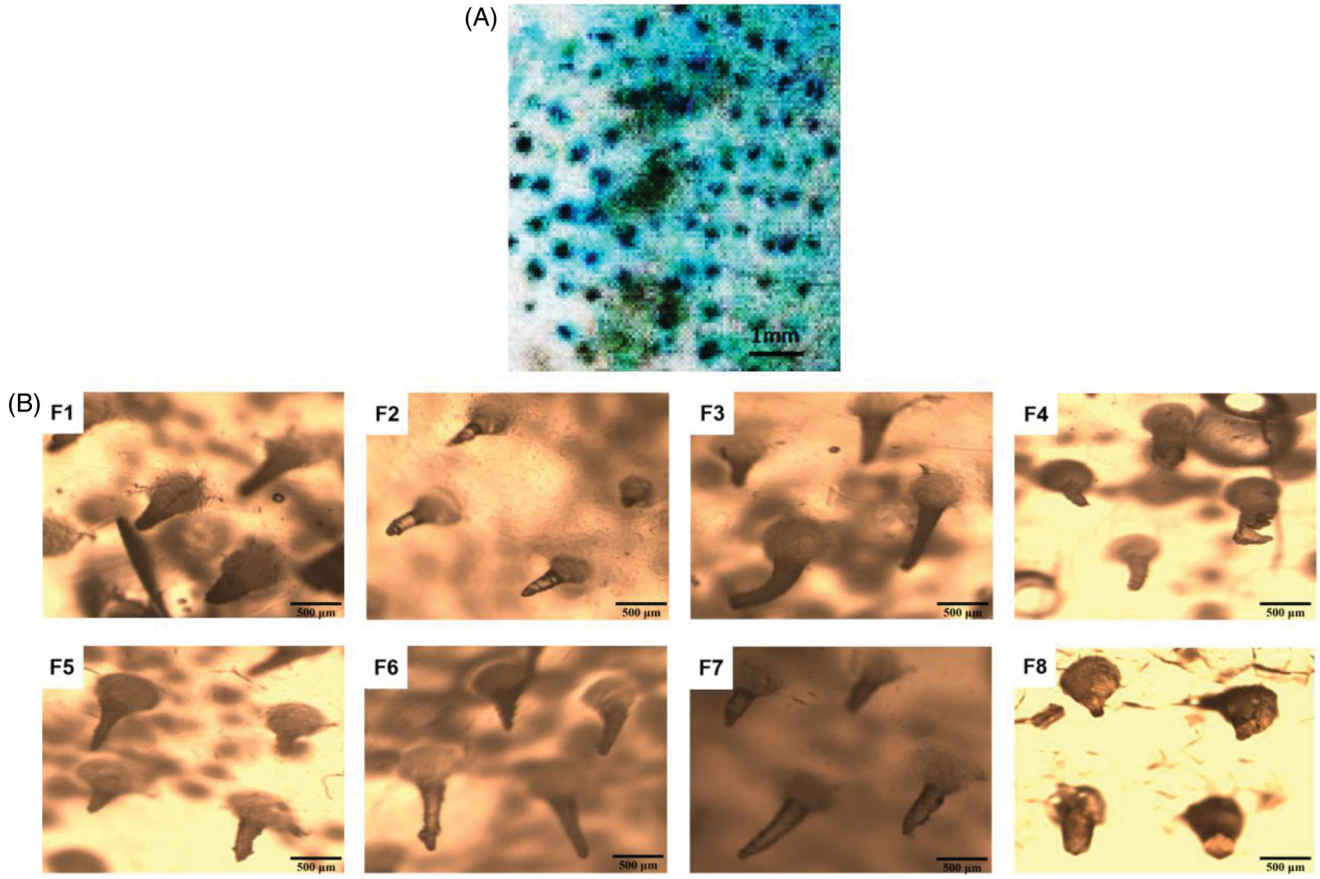

Figure 4. (A) Photograph of *in vitro* rat skin penetration with SH-MN; (B) F1–8 are micrographs of SH-MN prepared as different formulations after mechanical experiments.

curved. The length was not uniform, and the needle tips were not pointed.

3.2. Mechanical testing of SH-MN

As shown in Figure 4(A), the skin pierced by the MN was dyed blue, which indicated that the MN could successfully puncture rat skin. As can be seen from Figure 4(B), the MN of formulations F1, F2, F5, F6, and F7 were still intact. In contrast, there were some deformation and breakage for MN of with F3, F4, and F8. This also showed that the MN of formulations F1, F2, F5, F6, and F7 have good mechanical properties.

3.3. In vitro *diffusion studies*

SH content was determined by UHPLC, and the cumulative permeation amount (Q_n) was calculated according to the following formula. Subsequently, linear regression was performed on the cumulative permeation amount (Q_n) versus

time (t). The slope of the regression equation was the permeation rate (J_s), and the experimental results were processed and analyzed using statistical methods.

$$Q_n = \left(C_n V + V_0 \sum_{i=1}^{i=n-1} C_i \right) \Big/ S$$

where Q_n is the cumulative permeation per unit area of SH at the nth sampling point, C_n is the mass concentration of SH in the nth sampling point receiving the solution, and C_i is the mass concentration of SH in the liquid at the ith sampling point, V is the volume of the receiving pool (8 mL), V_0 is the sampling volume (1 mL), and S is the effective transmissive area (3.14 cm^2) of drug diffusion. The release curves are shown in Figure 5(A).

MN with the largest cumulative permeation amount and fastest release rate were prepared with formulation F7. Based on the results of comprehensive moldability and mechanical tests, the final formulation of SH-MN were as follows: PVP (50%), chondroitin sulfate (15%), and SH (35%); the amount of water added was ~50% of the total solids.

3.4. In vitro *percutaneous permeation of SH-MN and SH-G*

Figure 5(B) shows that the cumulative permeation and permeation rates of SH-MN were 5.31 and 5.06 times higher than that of SH-G, and the cumulative penetration of SH-MN was significantly different from SH-G ($p < .05$), indicating that SH-MN can significantly improve percutaneous penetration of SH.

3.5. In vivo *probe recovery experiment*

3.5.1. In vitro *recovery of microdialysis*

Increment and decrement methods were performed to examine the effect of different flow rates and concentrations on *in vitro* probe recovery. According to the results in Figure 5(C), the *in vitro* recovery of probes with both methods decreased with increasing flow rate but were similar at the same flow rate. Figure 5(D) indicates that when the perfusion rate was 1 μL min^{-1}, different concentrations of perfusate (1, 5, 10, and 20 μg mL^{-1}) had a minimal effect on probe recovery.

3.5.2. In vivo *recovery of microdialysis*

The results in Figure 5(E) show that the *in vivo* recovery of probes also decreased with higher flow rate. At different locations, the recovery in blood was greater than that in the skin. At different concentrations, probe recovery was not significantly different at the various flow rates and sampling positions, which indicated the concentration does not affect the recovery rate *in vivo* (Figure 5(F)). In addition, probe recovery in blood was greater than that for the skin.

3.5.3. *Pharmacokinetics detected via* in vivo *microdialysis*

The drug concentration-time profiles of SH in the skin after administration of two formulations are shown in Figure 5(G). SN concentration increased at a steady rate from 1 h. After reaching the peak, the drug concentration in the skin of the MN group decreased significantly, while the SH-G group decreased at a steady rate. The pharmacokinetic parameters in the skin showed that the peak concentrations (C_{max}) of the SH-G and SH-MN groups were 6.82 ± 0.20 μg mL^{-1} and 10.80 ± 0.43 μg mL^{-1}, respectively. It can be seen that the area under the curve ($AUC_{(0-t)}$) of the MN and SH-G groups were 1661.49 ± 7.76 μg·(mL min)$^{-1}$ and 2378.97 ± 58.68 μg·(mL min)$^{-1}$. The $AUC_{(0-t)}$ of the SH-MN group was 1.43 times that of the SH-G group, which indicated that dosing with MN remarkably improved the percutaneous properties of SH and enhanced its relative bioavailability (Table 2). The drug concentration-time curve in the blood showed that drug concentration in the SH-MN began to decrease after reaching the peak at ~40 min, while the SH-G group concentration decreased at a steady rate (Figure 5(H)).

The blood pharmacokinetic parameters showed the C_{max} of the SH-G and SH-MN groups were 3.15 ± 0.24 μg mL^{-1} and 6.80 ± 0.26 μg mL^{-1}, respectively. The AUC of the SH-MN group in the blood was 1.63 times that of the SH-G group. It indicated that under equal dosing conditions, the drug-loaded MN enhanced the percutaneous penetration effect of SH, which could improve SH relative bioavailability (Table 3).

3.6. In vivo *release behavior of SH-MN*

As shown in Figure 6(A–C), the tips of MN gradually dissolved and reduced after absorbing the tissue fluid. Almost the entire needle tip was dissolved 4 h after administration. The longitudinal section images taken 1 h after administration are shown in Figure 6(D–F). The skin surface exhibited inverted triangular channels, and the nuclei in the skin were successfully stained blue at the excitation wavelength of 405 nm. At the 488-nm excitation wavelength, SH (green fluorescence) was distributed around the skin surface and around the pores. Figure 6(G–I) show that SH distribution increased in the skin over time. The 4-h sample showed the highest fluorescence intensity, while in the 8 h sample, SH intensity decreased significantly and was distributed evenly throughout the skin.

The transverse sections are was shown in Figure 7, the distribution trend was similar to that observed in the longitudinal sections. The green fluorescence in the sample is centered in intense spots, and the fluorescent signal was low around these spots. Fluorescence was detected at a depth of 200 μm in the 4-h sample. There was no obvious spot in the 8-h sample, but green fluorescence could be detected in the skin at each depth.

According to Figure 6(A–C,G–I), the MN tips were almost completely dissolved within 4 h after administration. The SH content was the highest in the section observed for 4 h and was extensively distributed in the skin. This confirmed the previous result that the highest skin concentration of the drug was 4 h in the SH-MN group.

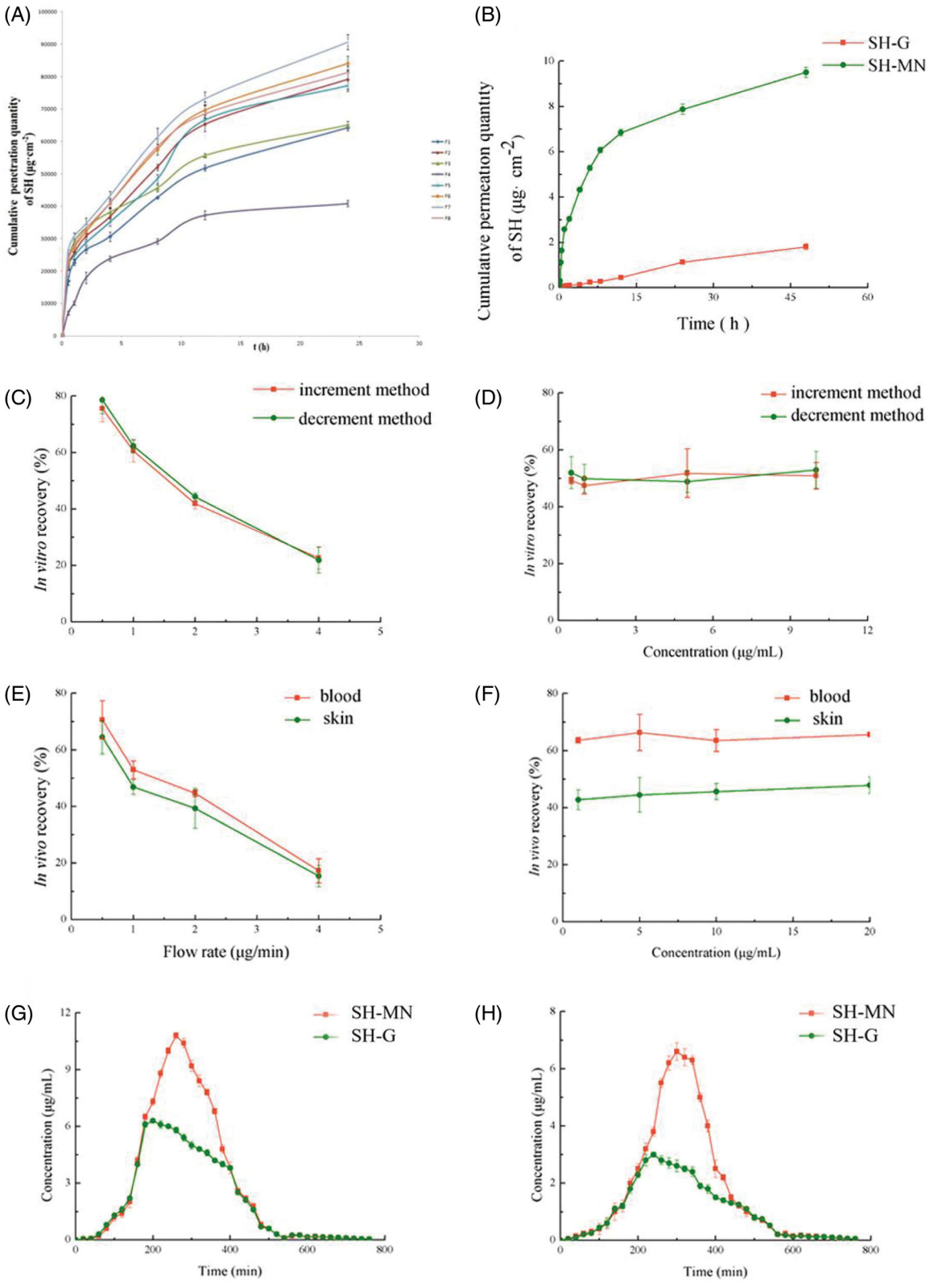

Figure 5. (A) *In vitro* cumulative permeation quantity of different formulations. (B) *In vitro* cumulative permeation quantity of SH from SH-G and SH-MN. (C) Effect of flow rate on *in vitro* recovery of microdialysis probes. (D) Effect of concentration on *in vitro* recovery of microdialysis probes. (E) Effect of flow rate on *in vivo* recovery of microdialysis probes. (F) Effect of concentration on *in vivo* recovery of microdialysis probes. (G) Concentration-time curves of SH in the skin and (H) blood (mean ± SD; $n = 5$).

4. Discussion

Due to the excellent anti-inflammatory, immunosuppressive properties, SH is commercially available for RA treatments in tablet, pill, or injection forms. Since many limitations are existed in oral and injectable formulations of SH, studies have been carried out on its topical dosage forms (Kim et al.,

2018). Previous publications have demonstrated that a topical gel with a drug content of 2% (w/w) had a good therapeutic effect for the treatment of arthritis (Ling et al., 2008; Shao, Zhou, Huang, et al., 2013; Shao, Zhou, & Zhou, 2013). However, ionic drugs generally encounter with poor percutaneous absorption performance due to cuticle barrier, it is crucial to improve their percutaneous absorption. In this study, the drug loading of SH-MN was 4% (w/w), which was an effective therapeutic amount for the treatment of arthritis.

Table 2. Pharmacokinetic parameters in skin (mean ± SD; $n = 5$).

PK parameters	SH-G	SH-MN
$T_{1/2\alpha}$ (min)	163.15 ± 2.64	188.54 ± 5.16
$T_{1/2\beta}$ (min)	101.67 ± 3.17	99.48 ± 3.65
T_{max} (min)	200	240
C_{max} (μg mL^{-1})	6.82 ± 0.20	10.80 ± 0.43*
AUC_{0-t}	1661.49 ± 7.76	2378.97 ± 58.68**
MRT_{0-t} (min)	270.04 ± 1.32	272.84 ± 1.15

SH-G, *$p < .05$; **$p < .01$.

Table 3. Pharmacokinetic parameters in blood (mean ± SD; $n = 5$).

PK parameters	SH-G	SH-MN
$T_{1/2\alpha}$ (min)	69.73 ± 3.28	108.49 ± 8.91*
$T_{1/2\beta}$ (min)	306.34 ± 5.87	383.98 ± 6.51*
T_{max} (min)	240	300
C_{max} (μg mL^{-1})	3.15 ± 0.24	6.80 ± 0.26**
AUC_{0-t}	813.47 ± 5.74	1327.53 ± 11.73*
MRT_{0-t} (min)	299.92 ± 2.74	306.68 ± 1.37

SH-G, *$p < .05$; **$p < .01$.

PVP is an ideal autolytic MN matrix material because of its good water solubility and biocompatibility. After being incorporated into MN to penetrate the skin, it can effectively absorb tissue fluid and promote drug dissolution without causing skin irritation (Ronnander et al., 2019). CS as a polysaccharide has good solubility and biocompatibility; it also increases MN mechanical strength (Ito et al., 2016).

In the MN preparation process, we assessed different drying methodss. When the vacuum oven was used for high-temperature drying, the MN often had cracks, difficulty in demolding, and poor moldability, which may have been due to uneven heating of the matrix material after casting. For these reasons, the method of air drying at room temperature was adopted. This method can be uniform and stable, but it is affected by air humidity, resulting in incomplete drying and difficulty in demolding. The cast matrix material was then placed in a desiccator to obtain the optimal mold release (Lee et al., 2011).

According to the drug concentration-time curve, the skin concentrations for the two formulations were similar in the

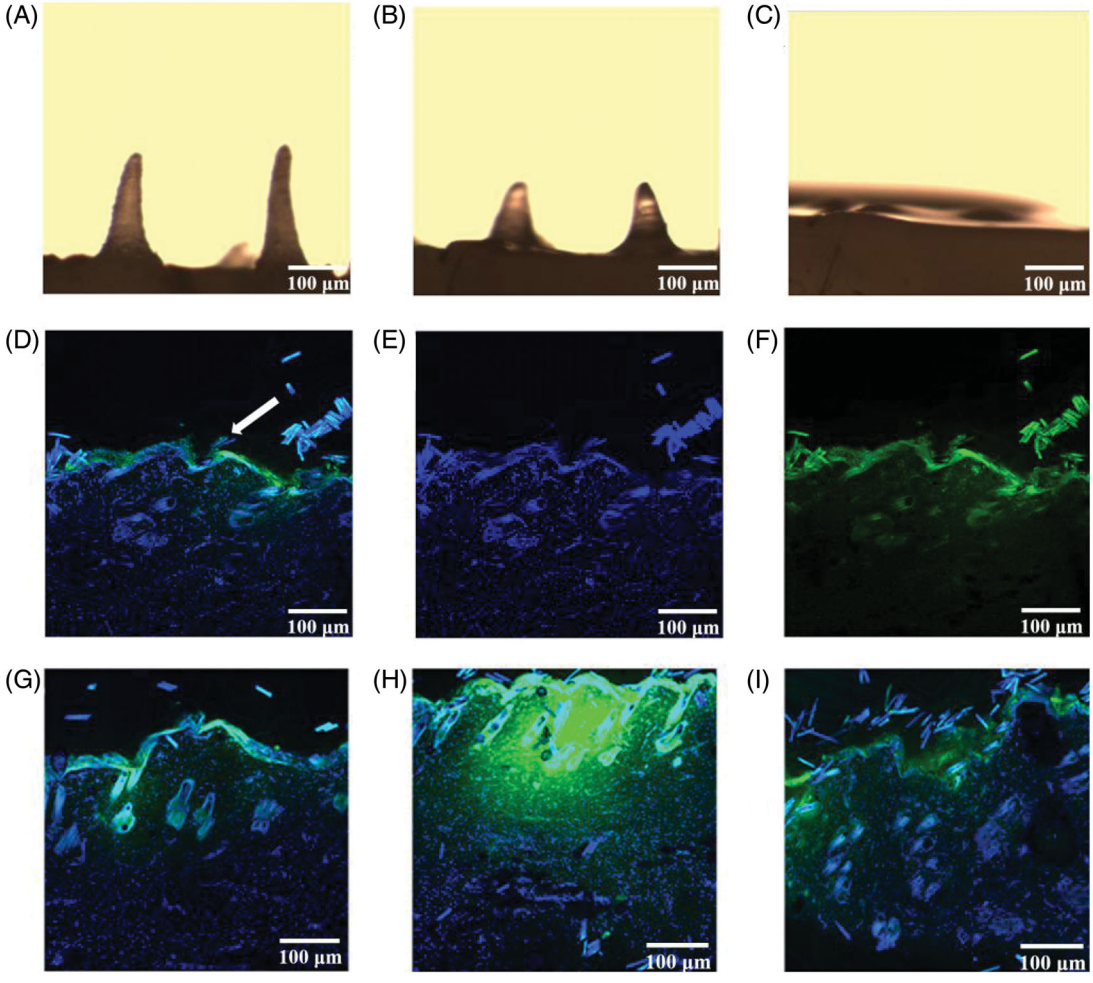

Figure 6. (A–C) MN morphology after administration for 1, 2, and 4 h. (D–F) Longitudinal sections of rat abdominal skin 1 h after administration with DAPI (D), SIN fluorescent labels (E), DAPI and SIN fluorescent labels (F). (G–I) Lengthwise section of rat abdominal skin after administration with DAPI and SIN fluorescent labels for 2, 4, and 8 h.

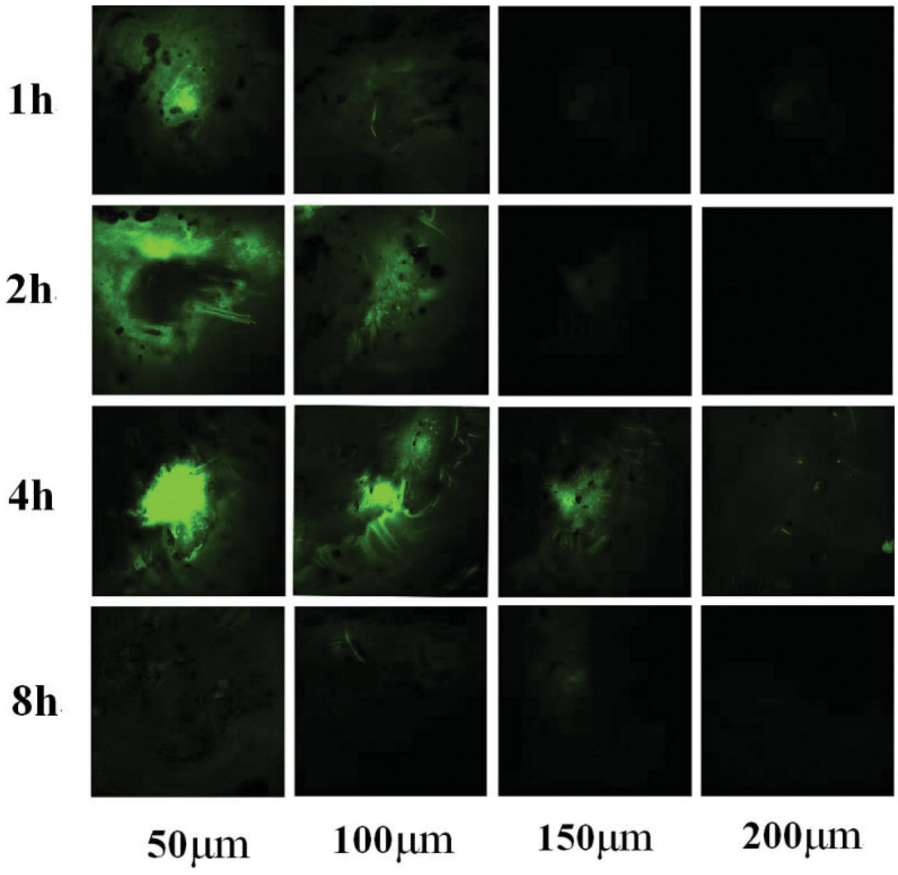

Figure 7. Transverse section of rat abdominal skin after administration for 1, 2, 4, and 8 h.

first 2 h, and blood concentrations were similar for the first 3 h. Moreover, the maximum skin and blood concentrations were higher in the SH-MN group compared to the SH-G group. *In vitro* permeation experiments showed that the cumulative permeation and permeation rate of the SH-MN group decreased to large extents relative to the Gel group. The possible reason was that the subcutaneous tissue fluid volume was excessively different from the PBS content in the receiving chamber *in vitro*. At the same time, the drug concentration of the SH-MN group rapidly decreased after reaching the peak, and the rate was faster than that in the SH-G group. This may be due to opening of the drug channel on the surface of the skin due to the release of the drug at the MN tips. We compared the mean residence times of the two types of dosages and observed a small difference, indicating that the sustained release effect of SH by MN administration is not much different from that of the gel.

Based on the length and size of the MN used here, it is speculated that MN should be able to produce micron-sized pores after piercing the skin. Figure 6(G–I), MN channel formation was not obvious, but green fluorescence was detected in the skin samples. There are two reasons why channels were not observed. One is that the sample was squeezed during sampling, and the frozen section was sliced, causing local deformation. Second, since the prepared MN tip distance is ~1 mm, the hole spacing after piercing should be similar. The prepared skin slice sample may miss the position of the channel. Future studies should consider the slice thickness according to MN tip spacing.

5. Conclusions

In this study, a novel SH-loaded MN was prepared using PVP and CS with a casting method. The transdermal pharmacokinetics and release mechanism results showed that the prepared MN have good mechanical properties and formability. Compared with the SH-G control, SH-MN significantly increased the cumulative permeability and permeability rates. Transdermal performance was markedly improved after the drug-loaded MN penetrated the skin. The tip of the needles could absorb the tissue fluid in the body, allowing the drug to release along the pores pierced through the skin and spread into the surrounding skin tissue. The drug was released about 4 h after MN application. The concentration of the drug in the skin was the largest, and the penetration depth under the skin was 200 μm. Thereafter, the drug accumulated in the skin tissue, was gradually absorbed by the body, and entered the blood system to circulate, achieving systemic administration. In conclusion, this study demonstrates the feasibility of dissolving MN patches to deliver SH and other biomolecules.

Disclosure statement

No potential conflict of interest was reported by the author(s).

Funding

This work was supported by the National Natural Science Foundation of China [81873019, 81274099]; and Research Projects of Top Talents in Anhui Province [2018D160].

References

Arya J, Henry S, Kalluri H, et al. (2017). Tolerability, usability and acceptability of dissolving microneedle patch administration in human subjects. Biomaterials 128:1–7.

Boopathy AV, Mandal A, Kulp DW, et al. (2019). Enhancing humoral immunity via sustained-release implantable microneedle patch vaccination. Proc Natl Acad Sci USA 116:16473–8.

Chang H, Zheng M, Yu X, et al. (2017). A swellable microneedle patch to rapidly extract skin interstitial fluid for timely metabolic analysis. Adv Mater 1702243.

Chen SY, Zou Y, Huang YQ, et al. (2017). Effects of sinomenine on proliferation and apoptosis of MCL Jeko-1 cell line and its mechanism. Zhongguo Shi Yan Xue Ye Xue Za Zhi 25:1675–9.

Fakhraei LS, Seo SH, Kim S, et al. (2018). Transcutaneous implantation of valproic acid-encapsulated dissolving microneedles induces hair regrowth. Biomaterials 167:69–79.

Fernandez-Garcia R, Lalatsa A, Statts L, et al. (2020). Transferosomes as nanocarriers for drugs across the skin: quality by design from lab to industrial scale. Int J Pharm 573:118817.

Gao B, Wu Y, Yang Y, et al. (2018). Sinomenine exerts anticonvulsant profile and neuroprotective activity in pentylenetetrazole kindled rats: involvement of inhibition of NLRP1 inflammasome. J Neuroinflammation 15:152.

Gao Z, Lin Y, Zhang P, et al. (2019). Sinomenine ameliorates intervertebral disc degeneration via inhibition of apoptosis and autophagy in vitro and in vivo. Am J Transl Res 11:5956–66.

Garcia A, Drown BS, Hergenrother PJ. (2016). Access to a structurally complex compound collection via ring distortion of the alkaloid sinomenine. Org Lett 18:4852–5.

Henry S, McAllister DV, Allen MG, et al. (1998). Microfabricated microneedles: a novel approach to transdermal drug delivery. J Pharm Sci 87: 922–5.

Hong X, Wei L, Wu F, et al. (2013). Dissolving and biodegradable microneedle technologies for transdermal sustained delivery of drug and vaccine. Drug Des Devel Ther 7:945–52.

Ita K. (2016). Transdermal iontophoretic drug delivery: advances and challenges. J Drug Target 24:386–91.

Ito Y, Inagaki Y, Kobuchi S, et al. (2016). Therapeutic drug monitoring of vancomycin in dermal interstitial fluid using dissolving microneedles. Int J Med Sci 13:271–6.

Jabbari N, Asghari MH, Ahmadian H, et al. (2015). Developing a commercial air ultrasonic ceramic transducer to transdermal insulin delivery. J Med Signals Sens 5:117–22.

Kaushik S, Hord AH, Denson DD, et al. (2001). Lack of pain associated with microfabricated microneedles. Anesth Analg 92:502–4.

Kim JH, Shin JU, Kim SH, et al. (2018). Successful transdermal allergen delivery and allergen-specific immunotherapy using biodegradable microneedle patches. Biomaterials 150:38–48.

Kim NW, Kim SY, Lee JE, et al. (2018). Enhanced cancer vaccination by in situ nanomicelle-generating dissolving microneedles. ACS Nano 12: 9702–13.

Kim NW, Lee MS, Kim KR, et al. (2014). Polyplex-releasing microneedles for enhanced cutaneous delivery of DNA vaccine. J Control Rel 179: 11–7.

Kiselmann C, Dobler D, Schmidts T, et al. (2018). Development of a skin-friendly microemulsion for dermal allergen-specific immunotherapy. Int J Pharm 550:463–9.

Lee K, Lee CY, Jung H. (2011). Dissolving microneedles for transdermal drug administration prepared by stepwise controlled drawing of maltose. Biomaterials 32:3134–40.

Ling J, Xie B, Wang Y, et al. (2008). Dynamic determination of sinomenine in skin by microdialysis. J Chin Med Mater 31:1062–4.

Liu J, Shao H, Fang S, et al. (2019). Evaluation of pharmacokinetics and pharmaco-dynamics of sinomenine-hyaluronic acid conjugate after intra-articular administration for osteoarthritis treatment. Drug Des Dev Ther 13:657–65.

Lopez-Ramirez MA, Soto F, Wang C, et al. (2020). Built-in active microneedle patch with enhanced autonomous drug delivery. Adv Mater 32:e1905740.

Ma G, Wu C. (2017). Microneedle, bio-microneedle and bio-inspired microneedle: a review. J Control Rel 251:11–23.

Pan Q, Wang S, Lu J, et al. (2010). Synthesis of N11-anchoring biotinylated artemisinin derivatives and their preliminary biological assessment. Sci China Chem 53:119–24.

Prausnitz MR, Langer R. (2008). Transdermal drug delivery. Nat Biotechnol 26:1261–8.

Romgens AM, Bader DL, Bouwstra JA, et al. (2015). Diffusion profile of macromolecules within and between human skin layers for (trans)dermal drug delivery. J Mech Behav Biomed Mater 50:215–22.

Ronnander JP, Simon L, Koch A. (2019). Transdermal delivery of sumatriptan succinate using iontophoresis and dissolving microneedles. J Pharm Sci 108:3649–56.

Shao JZ, Zhou L, Huang HR, Zhou YB. (2013). Study on the relationship of sinomenine concentration between the blood and the knee joint fluid in rabbit. China Med Herald 10:23.

Shao JZ, Zhou L, Zhou YB. (2013). Study on pharmacokinetic-pharmacodynamic characteristics of sinomenine in rabbits. Chin Acad J 24: 597–601.

Sullivan SP, Koutsonanos DG, Del PM, et al. (2010). Dissolving polymer microneedle patches for influenza vaccination. Nat Med 16:915–20.

Van Smeden J, Janssens M, Gooris GS, et al. (2014). The important role of stratum corneum lipids for the cutaneous barrier function. Biochim Biophys Acta 1841:295–313.

Wang J, Wei Y, Fei Y, et al. (2017). Preparation of mixed monoterpenes edge activated PEGylated transfersomes to improve the in vivo transdermal delivery efficiency of sinomenine hydrochloride. Int J Pharm 533:266–74.

Wu X, Chen Y, Gui S, et al. (2016). Sinomenine hydrochloride-loaded dissolving microneedles enhanced its absorption in rabbits. Pharm Dev Technol 21:787–93.

Xu J, Xu B, Tao J, et al. (2017). Microneedle-assisted, DC-targeted codelivery of pTRP-2 and adjuvant of paclitaxel for transcutaneous immunotherapy. Small 13:1700666.

Yin M, Xiao L, Liu Q, et al. (2019). 3D printed microheater sensor-integrated, Drug-Encapsulated microneedle patch system for pain management. Adv Healthcare Mater 8:1901170.

Zhao Z-J, Zhao C, Xiao J, Wang J-C. (2016). Transdermal permeation and anti-inflammation activities of novel sinomenine derivatives. Molecules 21:1520.